frontiers in Chemistry

ORIGINAL RESEARCH
published: 09 October 2018
doi: 10.3389/fchem.2018.00476

Lithium Sulfide–Carbon Composites via Aerosol Spray Pyrolysis as Cathode Materials for Lithium–Sulfur Batteries

Noam Hart[1], *Jiayan Shi*[1], *Jian Zhang*[2], *Chengyin Fu*[1] *and Juchen Guo*[1,2*]

[1] *Department of Chemical and Environmental Engineering, University of California, Riverside, Riverside, CA, United States,*
[2] *Materials Science and Engineering Program, University of California, Riverside, Riverside, CA, United States*

We demonstrate a new technique to produce lithium sulfide-carbon composite (Li_2S-C) cathodes for lithium-sulfur batteries *via* aerosol spray pyrolysis (ASP) followed by sulfurization. Specifically, lithium carbonate-carbon (Li_2CO_3-C) composite nanoparticles are first synthesized via ASP from aqueous solutions of sucrose and lithium salts including nitrate ($LiNO_3$), acetate (CH_3COOLi), and Li_2CO_3, respectively. The obtained Li_2CO_3-C composites are subsequently converted to Li_2S-C through sulfurization by reaction to H_2S. Electrochemical characterizations show excellent overall capacity and cycle stability of the Li_2S-C composites with relatively high areal loading of Li_2S and low electrolyte/Li_2S ratio. The Li_2S-C nanocomposites also demonstrate clear structure-property relationships.

Keywords: aerosol spray pyrolysis, nanocomposites, lithium-sulfur batteries, lithium sulfide, sulfurization

OPEN ACCESS

Edited by:
Fan Zhang,
Fudan University, China

Reviewed by:
Piercarlo Mustarelli,
University of Pavia, Italy
Yuan Yang,
Columbia University, United States

***Correspondence:**
Juchen Guo
jguo@engr.ucr.edu

Specialty section:
This article was submitted to Electrochemistry, a section of the journal Frontiers in Chemistry

Received: *20 July 2018*
Accepted: *20 September 2018*
Published: *09 October 2018*

Citation:
Hart N, Shi J, Zhang J, Fu C and Guo J (2018) Lithium Sulfide–Carbon Composites via Aerosol Spray Pyrolysis as Cathode Materials for Lithium–Sulfur Batteries. Front. Chem. 6:476. doi: 10.3389/fchem.2018.00476

INTRODUCTION

Lithium-sulfur (Li-S) batteries are regarded as one of the most promising electrochemical energy storage technologies due to their low cost, environmental benignity, and outstanding theoretical capacity (Wang et al., 2013; Son et al., 2015). However, despite tremendous research and development efforts, there are still a number of challenges hindering their commercialization. Among these key challenges are the polysulfides shuttle effect and high electrolyte/sulfur ratio, which are significantly magnified by the instability of the Li metal anode (Chen J. et al., 2017; Chen S. et al., 2017; Pan et al., 2018; Wu et al., 2018). Therefore, high capacity non-Li anodes, particularly those comprised of silicon-based materials, have been proposed as replacements for Li metal in Li-S batteries (Yang et al., 2010). The use of silicon anode materials would require a pre-lithiated sulfur cathode, i.e., lithium sulfide (Li_2S). In recent years, various methods to synthesize Li_2S-carbon composite materials have been reported, including high-energy mixing Li_2S with carbon (Cai et al., 2012; Jha et al., 2015), chemical lithiation of S-C composites (Hwa et al., 2015), Li_2S-C composites synthesis *via* dissolving and precipitating Li_2S in ethanol (Wu et al., 2014a,b,c, 2015, 2016), embedding Li_2S in carbon matrix *via* Li-nitrogen interaction (Guo et al., 2013), reaction between Li metal and carbon disulfide (Tan et al., 2017), converting LiOH to Li_2S *via* sulfurization with H_2S (Dressel et al., 2016), and thermal reduction of Li_2SO_4 by carbon (Yang et al., 2013; Kohl et al., 2015; Li et al., 2015; Yu et al., 2017; Zhang et al., 2017; Ye et al., 2018). In addition, the mechanism studies on Li_2S activation and capacity degradation were also reported (Vizintin et al., 2017; Piwko et al., 2018). In this work, we report a new scalable method for synthesizing Li_2S-C composites via aerosol spray pyrolysis (ASP) followed by sulfurization.

MATERIALS AND METHODS

Materials Synthesis

Three lithium salts including lithium nitrate ($LiNO_3$), lithium acetate (CH_3COOLi) and lithium carbonate (Li_2CO_3) were used as the precursors for Li_2S with sucrose as the precursor for carbon. Each Li salt was dissolved in deionized water with sucrose at different concentrations as listed in **Table S1**. The obtained solutions were used in the ASP process.

The ASP system in this study is illustrated in **Figure S1**. The commercial aerosol generator (TSI, Model 3076) consisting of a nebulizer and a solution reservoir is attached to a diffusion dryer followed by a tubular furnace and a filter collector. The diffusion dryer was composed by two concentric tubes: The outer tube is made of 3-inch inner diameter PVC tubing and the inner tube is made of 0.5-inch diameter steel mesh with the annular space filled with porous silica gel. The aerosol of the precursor solution was generated by the nebulizer and carried through the diffusion dryer by argon gas to desiccate the water content. The resultant dry particles were continuously carried into the tube furnace heated at 850°C to produce the Li_2CO_3-C nanoparticles, which are collected with a stainless-steel filter down stream outside the tube furnace.

The synthesized Li_2CO_3-C composite is placed in an alumina boat in a tubular furnace, followed by purging with argon for an hour. The furnace was then heated to 725°C and maintained at this temperature for 5 h under a flow of 5 vol.% H_2S and 95 vol.% argon. After 5 h the flow gas was switched to pure argon and the furnace was cooled naturally to room temperature. The product was collected in an argon-filled glovebox due to the sensitivity of Li_2S to moisture.

Materials Characterization

The nitrogen adsorption-desorption isotherms of the produced composite materials were obtained with a surface area and porosity analyzer (Micromeritics ASAP2020). For a particular analysis, approximately 200 mg sample was first degassed at 150°C for 3 h, then the nitrogen adsorption-desorption isotherms were measured from 0 to 1 relative pressure. The surface area was obtained with the Brunauer-Emmett-Teller (BET) method. The crystalline species in the composites were characterized by powder X-Ray diffraction (XRD, PANalytical) with a CuKα source and a scan rate of $0.11^\circ\ s^{-1}$. Kapton tape was used to seal the Li_2S-C composites to protect Li_2S from reacting with the moisture in ambient environment during measurement. The morphology and microstructure of the composites were characterized by scanning electron microscopy (SEM) and transmission electron microscopy (TEM, Tecnai T12). Carbon content in the Li_2CO_3-C composites was measured with thermogravimetric analysis (TGA, TA Instruments). The TGA samples were held at 120°C for 30 min to remove the moisture absorbed from environment, followed by heating to 600°C at a rate of $10°C\ min^{-1}$ with an isothermal step in dry air. The carbon contents in Li_2CO_3-C_{NitS}, Li_2CO_3-C_{AceS} and Li_2CO_3-C_{CarS} (**Figure S2**) are very consistent at 20.7, 22.8, and 21.2 wt.%, respectively. Assuming complete conversion from Li_2CO_3 to Li_2S without carbon loss, the Li_2S content in Li_2S-C_{NitS}, Li_2S-C_{AceS} and Li_2S-C_{CarS} can be estimated as 70.4, 67.8, and 69.8 wt.%, respectively. The accurate Li_2S content in the Li_2S-C composites is determined as follows: 100 mg Li_2S-C was thoroughly washed 4 times using 15 mL ethanol each time in the glovebox to remove Li_2S. The obtained carbon was weighed after dried at 120°C for 8 h in the glovebox. The Li_2S content is 71.3 wt.% in Li_2S-C_{NitS}, 69.1 wt.% in Li_2S-C_{AceS}, and 71.6 wt.% in Li_2S-C_{CarS}, which all agree very well with the estimated values.

Electrode Preparation and Cell Testing

The electrode is composed of 80 wt.% of Li_2S-C composite, 10 wt.% of carbon black additive, and 10 wt.% of polystyrene as the binder. Polystyrene was selected as the binder to avoid the use of polar solvents (both protic and aprotic), most of which dissolve Li_2S to some extent. Instead, mesitylene (Sigma-Aldrich) was used as the solvent for polystyrene in the electrode slurry. The electrodes were coated on carbon-coated aluminum current collector (MTI Corporation) in the argon-filled glovebox, with the average loading of Li_2S-C composite at $2\ mg\ cm^{-2}$. The electrodes were dried overnight in argon glovebox at room temperature, followed by drying at 120°C for 4 h. The dried electrodes are assembled into 2032-type coin cells with lithium foil anode (99.9%, Alfa Aesar) and Celgard® 2,500 separator. The electrolyte used in this study is 1M lithium bis(trifluoromethanesulfonyl)imide (LiTFSI) solution in a mixture of 1,3-dioxolane (DOL), dimethoxyethane (DME) and 1-butyl-1-methylpyrrolidinium bis(trifluoromethanesulfonyl)imide (Pyr14TFSI) (1:3:1 by vol.) with 1.5 wt.% of $LiNO_3$. The electrolyte to Li_2S ratio (μL/mg) was kept at 10 in all coin cells testing. To activate the Li_2S-C electrode, the first anodic scan in the cyclic voltammetry (CV) was to 3.9 V vs. Li^+/Li, and the anodic limit in the following scans was 2.6 V vs. Li^+/Li. Similarly, the first charge was run at a rate of $50\ mA\ g^{-1}$ (with respect to Li_2S) to a charge cutoff of 3.5 V. Subsequent cycles are run at $117\ mA\ g^{-1}$ between 2.6 V and 1.8 V vs. Li^+/Li.

RESULTS AND DISCUSSION

During ASP synthesis, three aqueous solutions containing sucrose (as carbon precursor) and either lithium nitrate ($LiNO_3$), lithium acetate (CH_3COOLi), or lithium carbonate (Li_2CO_3), denoted as NitS, AceS, and CarS, respectively, were atomized into aerosols with a pressure-enabled atomizer. The aerosols were subsequently carried by argon gas through a diffusion dryer and a tubular furnace for pyrolysis within an inert environment. The powder X-ray diffraction (XRD) patterns in **Figure 1A** clearly indicate that the obtained composites from all three lithium salts are Li_2CO_3-C composite with comparable carbon content (20.7 wt.% in Li_2CO_3-C_{NitS}, 22.8 wt.% in Li_2CO_3-C_{AceS} and 21.2 wt.% in Li_2CO_3-C_{CarS} *via* thermalgravimetric analysis, **Figure S2**). It is worth noting that sucrose solution without the lithium salts (i.e., precursors of Li_2CO_3) completely decomposes during the same ASP without any carbon formation. This observation reveals that Li_2CO_3 serves as the nucleation sites for carbonization of sucrose in ASP (Skrabalak and Suslick, 2006). However, the formation mechanisms of Li_2CO_3 from these three Li salts are clearly

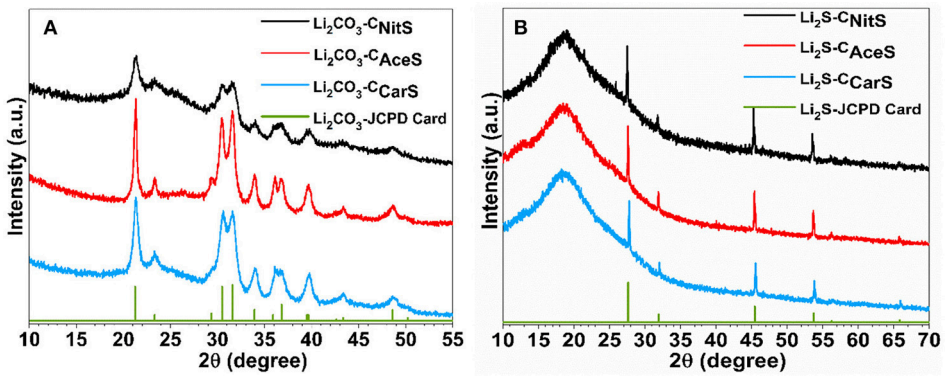

FIGURE 1 | XRD patterns of **(A)** the Li_2CO_3-C composites obtained from ASP and **(B)** the Li_2S-C composites after sulfurization.

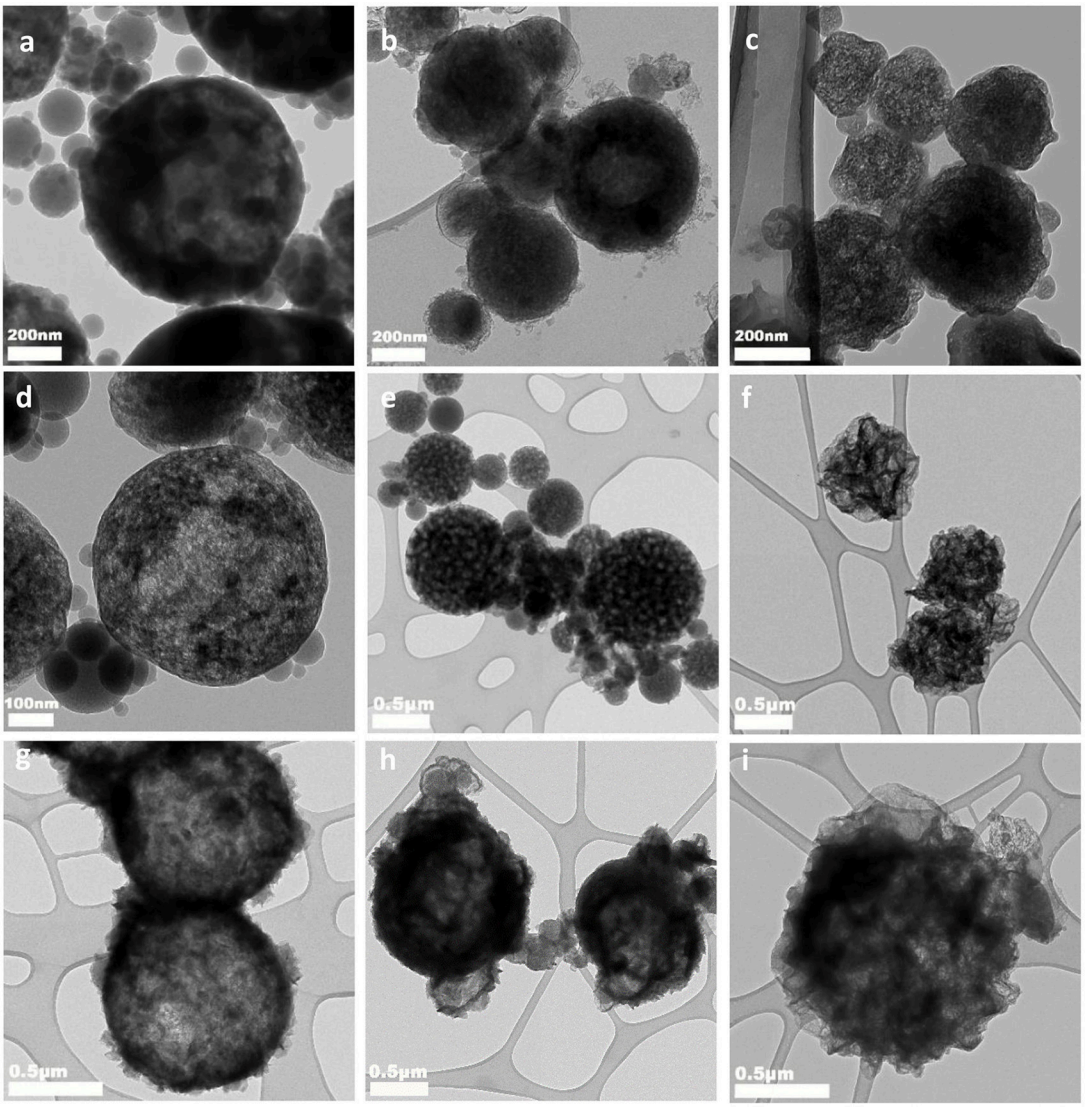

FIGURE 2 | TEM images of **(a)** Li_2CO_3-C_{NitS}, **(b)** Li_2CO_3-C_{AceS}, **(c)** Li_2CO_3-C_{CarS}; TEM images of the carbon matrix of **(d)** Li_2CO_3-C_{NitS}, **(e)** Li_2CO_3-C_{AceS}, **(f)** Li_2CO_3-C_{CarS} after Li_2CO_3 removed; and TEM images of **(g)** Li_2S-C_{NitS}, **(h)** Li_2S-C_{AceS}, **(i)** Li_2S-C_{CarS}.

different. For $LiNO_3$, its thermal decomposition is known to proceed according to **Reaction 1**: (Stern and Weise, 1969)

$$\mathbf{2LiNO_3 \rightarrow Li_2O + 2NO_x + (2.5 - x)O_2} \quad (1)$$

Based on the XRD evidence of Li_2CO_3 with the absence of crystalline Li_2O, it can be speculated that carbon dioxide (CO_2) released from pyrolysis of sucrose further reacts with Li_2O to generate Li_2CO_3 according to **Reaction 2**:

$$\mathbf{Li_2O + CO_2 \rightarrow Li_2CO_3} \quad (2)$$

CH_3COOLi undergoes thermal decomposition to generate Li_2CO_3 and acetone according to **Reaction 3**: (Roe and Finlay, 1952)

$$\mathbf{2CH_3COOLi \rightarrow Li_2CO_3 + C_3H_6O} \quad (3)$$

For the CarS precursor, Li_2CO_3 undergoes precipitation during ASP without decomposition, thus becoming directly embedded into the carbon matrix formed by the carbonization of sucrose.

Although the obtained Li_2CO_3-C composites have consistent composition and carbon content, they have distinctively different microstructures as displayed by the transmission electron microscopy (TEM) images in **Figure 2** (scanning electron microscopy images in **Figure S3**). The Li_2CO_3-C_{NitS} nanoparticles in **Figure 2A** have a hollow-shell structure with irregular-shaped interior voids due to the release of NO_x and O_2 gases during pyrolysis. The high solubility of $LiNO_3$ in water also contributes to the formation of this hollow structure. When water evaporates during ASP, $LiNO_3$ precipitates at the outer surface of the aerosol droplets following the surface precipitation mechanism (Messing et al., 1993). The microstructure of the Li_2CO_3-C_{NitS} nanoparticles is further revealed by the TEM image in **Figure 2D**, after the removal of Li_2CO_3 using diluted hydrochloric acid (HCl). The carbon matrix of Li_2CO_3-C_{NitS} has a highly porous structure after Li_2CO_3 removal, indicating that Li_2CO_3 occupies the majority of the volume in the Li_2CO_3-C_{NitS} nanoparticles. The specific surface area of Li_2CO_3-C_{NitS} before and after Li_2CO_3 removal obtained from the nitrogen adsorption-desorption isotherms (**Figure 3** and **Table S2**) is consistent with this observation: the specific surface area of Li_2CO_3-C_{NitS} is significantly increased from 26.8 to 608.2 $m^2\ g^{-1}$ after Li_2CO_3 removal.

On the other hand, Li_2CO_3-C_{AceS} nanoparticles show a denser spherical structure in **Figure 2B**. It is worth noting that the AceS precursor solution has a significantly lower sucrose/lithium salt molar ratio at 1:15 compared to 1:1.5 in NitS and 1:1.18 in CarS. Given the 22.8 wt.% carbon content in Li_2CO_3-C_{AceS}, it is believed the generated acetone during the pyrolysis of CH_3COOLi must function as the major source for carbon formation. The TEM image of the carbon matrix after Li_2CO_3 removal in **Figure 2E** reveals the distribution of Li_2CO_3 in the Li_2CO_3-C_{AceS} nanoparticles is not as uniform as in Li_2CO_3-C_{NitS}. The carbon matrix has a golf ball-like structure with relatively large pores, previously occupied by Li_2CO_3, distributed within. The specific surface area of Li_2CO_3-C_{AceS} is 76.3 $m^2\ g^{-1}$, which increases to 184.9 $m^2\ g^{-1}$ after Li_2CO_3 removal. This modest increase of surface area also indicates the relatively larger size of Li_2CO_3 compared to that of Li_2CO_3-C_{NitS}.

As shown in **Figure 2C**, the Li_2CO_3-C_{CarS} nanoparticles clearly have a different structure resembling crumpled spheres, which is due to the much lower solubility of Li_2CO_3 in water than those of $LiNO_3$ and CH_3COOLi. The concentration of Li_2CO_3 in the CarS precursor solution is 0.1 M, which is close to saturation (Zou et al., 2013). Therefore, Li_2CO_3 undergoes fast and uniform precipitation from the aerosol droplets' evaporation in ASP according to the volume precipitation mechanism (Messing et al., 1993). In addition, the ASP of CarS precursor also releases fewer gaseous species without decomposition of Li_2CO_3. Both factors contribute to better confinement and more uniform distribution of Li_2CO_3. After Li_2CO_3 removal, the carbon matrix retains its original structure with apparently higher porosity as shown in **Figure 2F**. The specific surface area of Li_2CO_3-C_{CarS} nanoparticles is 43.7 $m^2\ g^{-1}$, which increases to 443.6 $m^2\ g^{-1}$ after Li_2CO_3 removal.

The Li_2CO_3-C nanoparticles obtained *via* ASP were subsequently reacted with mixed hydrogen sulfide and argon gas (H_2S/Ar at 5/95 vol.%) at 725°C to yield the Li_2S-C composites

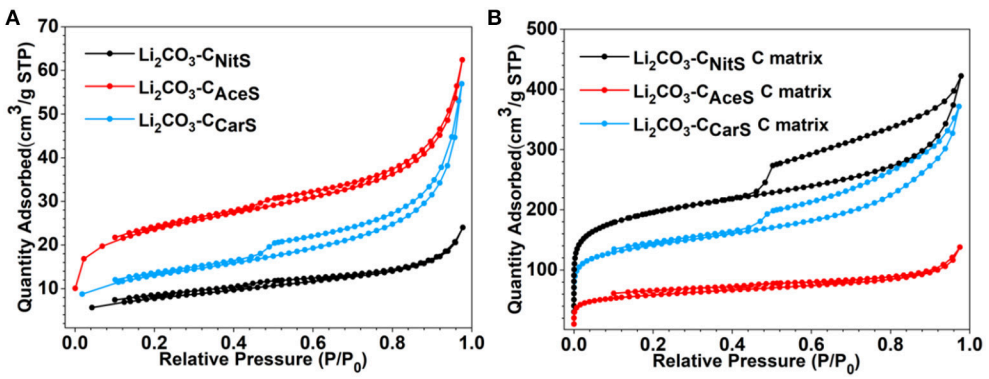

FIGURE 3 | N_2 adsorption-desorption isotherms of **(A)** Li_2CO_3-C nanoparticles and **(B)** the carbon matrix after Li_2CO_3 removal.

according to **Reaction 4**, confirmed by the XRD patterns shown in **Figure 1B**.

$$Li_2CO_3 + H_2S \rightarrow Li_2S + H_2O + CO_2 \quad (4)$$

The TEM images of the Li_2S-C composites in **Figures 2G–I** (scanning electron microscopy images in **Figure S4**) demonstrate that these nanoparticles sustain their original structures after the conversion to Li_2S from Li_2CO_3.

Figure 4 shows the first three CV cycles of the Li_2S-C vs. Li counter/reference electrode in two-electrode cells. The cathodic peak in the first delithiation scan of Li_2S-C_{NitS} is centered at 3.5 V with a small shoulder at 3.4 V. The Li_2S-C_{AceS} composite demonstrates a broader delithiation peak at the same potential.

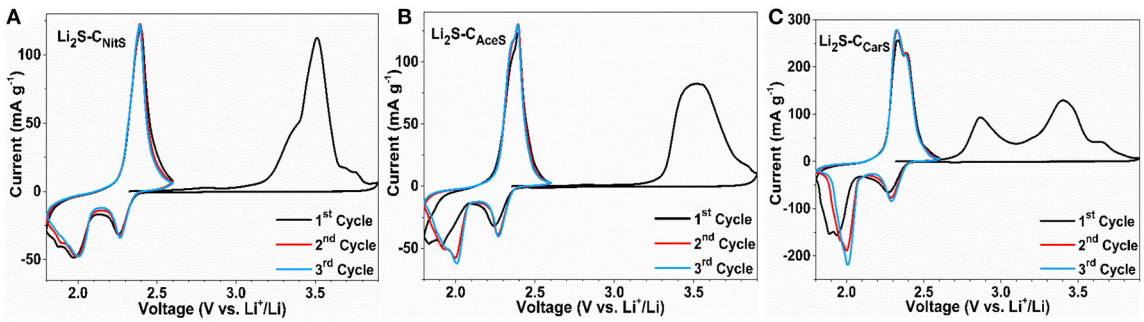

FIGURE 4 | CV scans of **(A)** Li_2S-C_{NitS}, **(B)** Li_2S-C_{AceS}, **(C)** Li_2S-C_{CarS} using 0.2 mV s^{-1} scan rate.

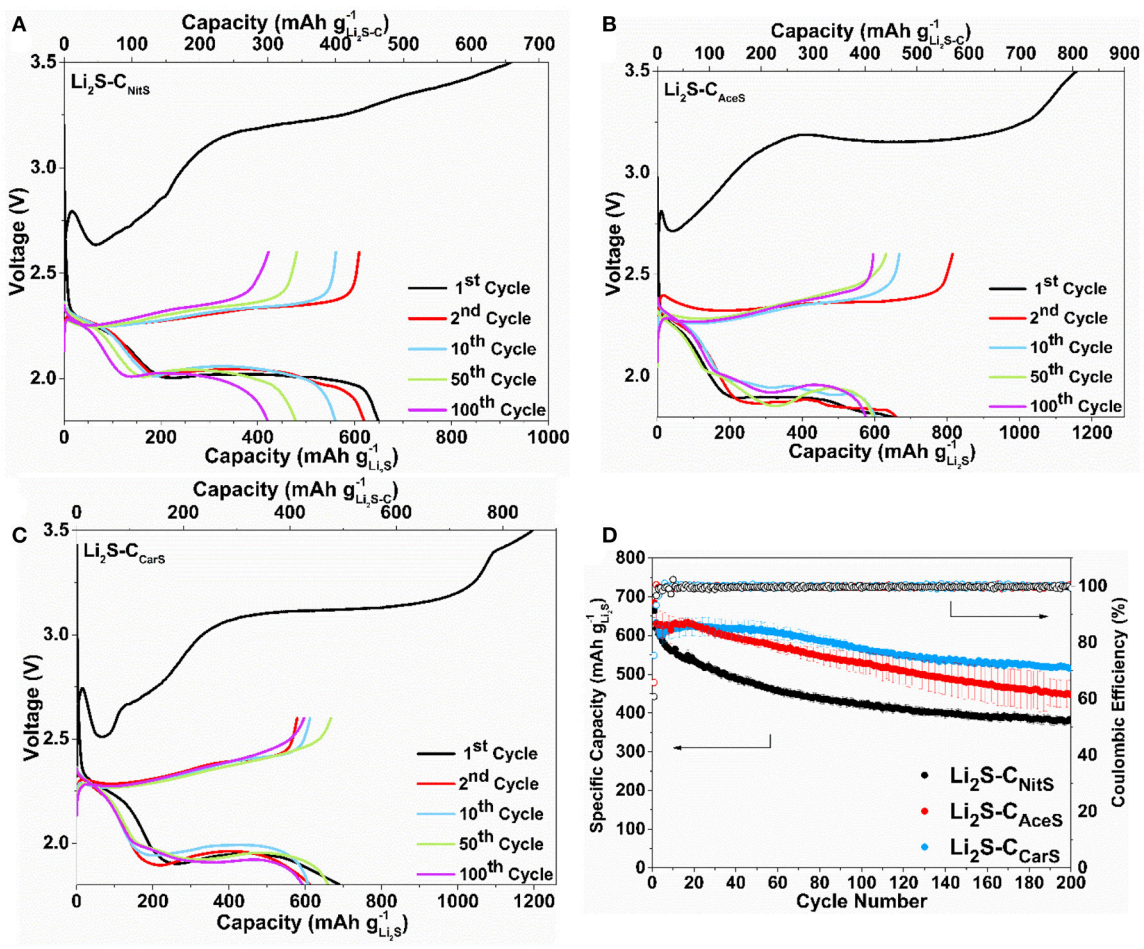

FIGURE 5 | Representative charge-discharge curves of **(A)** Li_2S-C_{NitS}, **(B)** Li_2S-C_{AceS}, **(C)** Li_2S-C_{CarS} at the 1st, 2nd, 10th, 50th, and 100th cycle, and **(D)** the cycle stability of these composites at 117 mA g^{-1}.

In contrast, Li_2S-C_{CarS} shows two distinct cathodic peaks at 2.75 and 3.4 V vs. Li^+/Li. The lower cathodic peak of the Li_2S-C_{CarS} composite at 2.75 V indicates a lower energy barrier for the delithiation reaction (Zhou et al., 2017). The Li_2S-C_{CarS} composite also demonstrates the highest peak current in the consecutive lithiation-delithiation scans. The superior performance of Li_2S-C_{CarS} may be reflective of the intimate contact of Li_2S and the carbon matrix. **Figure 5** displays the representative charge-discharge curves and the cycle stability of the Li_2S-C composites. The electrolyte/Li_2S ratio is 10:1 (μL/mg), and all Li_2S-C composites are first charged to 3.5 V (activation) vs. Li^+/Li with a current density of 50 mA g^{-1}. The charge-discharge curves demonstrate similar cycling behavior of these three Li_2S-C composites. However, Li_2S-C_{AceS} shows the highest charge-discharge hysteresis, which is consistent with the lowest surface area of its carbon matrix. On the other hand, although Li_2S-C_{NitS} shows the lowest voltage hysteresis due to the highest surface area of its carbon matrix, its capacity rapidly fades. As a composite with the balanced microstructure, Li_2S-C_{CarS} demonstrates the best overall performance: After 200 cycles, Li_2S-C_{CarS} can retain a capacity of 540 mAh g^{-1}, superior to 385 mAh g^{-1} of Li_2S-C_{NitS} and 460 mAh g^{-1} of Li_2S-C_{AceS}, indicating the effectiveness of the Li_2S-C_{CarS} composite architecture in sequestrating polysulfides. The overall performance demonstrated by Li_2S-$C_{CarS,}$ in terms of areal loading, E/Li_2S ratio, overall capacity, and cycle stability, is on par with the best performance reported to date (**Table S3**).

In summary, we examined a new synthetic route for the production of Li_2S-C composite materials for Li-S batteries. The combination of aerosol spray pyrolysis and sulfurization has been shown to be a robust method for the conversion of various lithium salts including nitrate, acetate, and carbonate to Li_2S-C nanocomposites using sucrose as the carbon precursor. Furthermore, the cycling performance of the Li_2S-C composite has been found to be closely correlated to its precursor-derived microstructure. The combination of Li_2CO_3 and sucrose results in the Li_2S-C composite with the best electrochemical performance, which has a non-hollow composite structure with Li_2S uniformly embedded in the carbon matrix. The detailed mechanism of aerosol spray pyrolysis and the optimization of the composite's structure and electrochemical performance will be further investigated in our future studies.

AUTHOR CONTRIBUTIONS

NH completed most of the experiments. JS, JZ, and CF helped with the experiments and data analysis. JG designed the experiments. All authors co-wrote the manuscript.

ACKNOWLEDGMENTS

We gratefully acknowledge the financial support from Power Energy Solutions Inc.

SUPPLEMENTARY MATERIAL

The Supplementary Material for this article can be found online at: https://www.frontiersin.org/articles/10.3389/fchem.2018.00476/full#supplementary-material

REFERENCES

Cai, K., Song, M., Cairns, J. E., Zhang, Y. (2012). Nanostructured Li_2S-C composites as cathode material for high-energy Lithium/Sulfur batteries. *Nano Lett*. 12, 6474–6479. doi: 10.1021/nl303965a

Chen, J., Henderson, W. A., Pan, H., Perdue, R. B., Cao, R., Hu, J. Z., et al. (2017). Improving Lithium–Sulfur battery performance under lean electrolyte through nanoscale confinement in soft swellable gels. *Nano Lett*. 17, 3061–3067. doi: 10.1021/acs.nanolett.7b00417

Chen, S., Gao, Y., Yu, Z., Gordin, L. M., Song, J., and Wang, D. (2017). High capacity of Lithium-Sulfur batteries at low electrolyte/Sulfur ratio enabled by an Organosulfide containing electrolyte. *Nano Energy* 31, 418–423. doi: 10.1016/j.nanoen.2016.11.057

Dressel, B. C., Jha, H., Eberle, A., Gasteiger, A. H., and Fassler, F. T. (2016). Electrochemical performance of Lithium-Sulfur batteries based on a Sulfur cathode obtained by H_2S gas treatment of a Lithium salt. *J. Power Sour*. 307, 844–848. doi: 10.1016/j.jpowsour.2015.12.140

Guo, J., Yang, Z., Yu, Y., Abruña, H. D., and Archer, L. A. (2013). Lithium–Sulfur battery cathode enabled by Lithium–Nitrile interaction. *J. Am. Chem. Soc*. 135, 763–767. doi: 10.1021/ja309435f

Hwa, Y., Zhao, J., and Cairns, E. J. (2015)Lithium Sulfide (Li2S)/Graphene Oxide nanospheres with conformal carbon coating as a high-rate, long-life cathode for Li/S cells. *Nano Lett*. 15, 3479–3486. doi: 10.1021/acs.nanolett.5b00820

Jha, H., Buchberger, I., Cui, X., Meini, S., and Gasteiger, H. A. (2015). Li-S batteries with Li2S cathodes and Si/C anodes. *J. Electochem. Soc*. 162, 1829–1835. doi: 10.1149/2.0681509jes

Kohl, M., Bruckner, J., Bauer, I., Althues, H., and Kaskel, S. (2015). Synthesis of highly electrochemically active Li2S nanoparticles for Lithium–Sulfur-batteries. *J. Mater. Chem. A* 3, 16307–16312. doi: 10.1039/C5TA04504E

Li, Z., Zhang, S., Zhang, C., Ueno, K., Yasuda, T., Tatara, R., et al. (2015). One-pot pyrolysis of Lithium Sulfate and graphene nanoplatelet aggregates: *in situ* formed Li2S/ graphene composite for Lithium–Sulfur batteries. *Nanoscale* 7, 14385–14392. doi: 10.1039/C5NR03201F

Messing, G., Zhang, S., and Jayanthi, G. (1993). Ceramic powder synthesis by spray pyrolysis. *J. Am. Ceram. Soc*. 76, 2707–2726.

Pan, H., Han, S. K., Engelhard, H. M., Cao, R., Chen, J., Zhang, J., et al. (2018). Addressing passivation in Lithium–Sulfur battery under lean electrolyte condition. *Adv. Funct. Mater*. 28:1707234. doi: 10.1002/adfm.201707234

Piwko, M., Weller, C., Hippauf, F., Dorfler, S., Althues, H., and Kaskel, S. (2018). Symmetric Lithium Sulfide-Sulfur cells: a method to study degradation mechanisms of cathode, separator and electrolyte concepts for Lithium-Sulfur batteries. *J. Electrochem. Soc*. 165, A1084–A1091. doi: 10.1149/2.1131805jes

Roe, A., and Finlay, J. B. (1952). The isotope effect II, pyrolysis of Lithium Acetate 1-C14. *J. Am. Chem. Soc*. 74, 2442–2443.

Skrabalak, S. E., and Suslick, K. S. (2006). Porous carbon powders prepared by ultrasonic spray pyrolysis. *J. Am. Chem. Soc*. 128, 12642–12643. doi: 10.1021/ja064899h

Son, Y., Son, Y., Lee, J., Jang, J., and Cho, J. (2015). Recent advances in Lithium Sulfide cathode materials and their use in Lithium Sulfur batteries. *Adv. Energy Mat*. 5:1500110. doi: 10.1002/aenm.201500110

Stern, K. H., and Weise, E. L. (1969). *High Temperature Properties and Decomposition of Inorganic Salts; Part 2. Carbonates*. Washington, DC: United States Dept of Commerce.

Tan, G., Xu, R., Xing, Z., Yuan, Y., Lu, J., Wen, J., et al. (2017). Burning lithium in CS2 for high-performing compact Li2 S–graphene nanocapsules for Li–S batteries. *Nat. Energy* 2:17090. doi: 10.1038/nenergy.2017.90

Vizintin, A., Chabanne, L., Tchernychova, E., Arcon, I., Stievano, L., Aquilanti, G., et al. (2017). The mechanism of Li_2S activation in Lithium-sulfur batteries: can we avoid the Polysulfide formation? *J. Power Sour*. 344, 208–217. doi: 10.1016/j.jpowsour.2017.01.112

Wang, D., Zeng, Q., Zhou, G., Yin, L., Li, F., Cheng, H., et al. (2013). Carbon-Sulfur composites for Li-S batteries: status and prospects. *J. Mat. Chem. A* 1, 9382–9394. doi: 10.1039/C3TA11045A

Wu, F., Kim, H., Magasinski, A., Lee, J., Lin, H., and Yushin, G. (2014a). Harnessing steric separation of freshly nucleated Li2S nanoparticles for bottom-up assembly of high-performance cathodes for Lithium-Sulfur and Lithium-Ion batteries. *Adv. Energy Mater*. 4:1400196. doi: 10.1002/aenm.201400196

Wu, F., Lee, J., Magasinski, A., Kim, H., and Yushin, G. (2014b). Solution-based processing of graphene-Li2S composite cathodes for Lithium-Ion and Lithium-Sulfur batteries. *Part. Part. Syst. Charact*. 31, 639–644. doi: 10.1002/ppsc.201300358

Wu, F., Lee, J., Zhao, E., Zhang, B., and Yushin, G. (2016). Graphene–Li2S–carbon nanocomposite for Lithium–Sulfur batteries. *ACS Nano* 10, 1333–1340. doi: 10.1021/acsnano.5b06716

Wu, F., Lee, J. E., Fan, F., Nitta, N., Kim, H., Zhu, T., et al. (2015). A hierarchical particle–shell architecture for long-term cycle stability of Li2S cathodes. *Adv. Mater*. 27, 5579–5586. doi: 10.1002/adma.201502289

Wu, F., Magasinski, A., and Yushin, G. (2014c). Nanoporous Li2S and MWCNT-linked Li2S powder cathodes for Lithium-Sulfur and Lithium-ion battery chemistries. *J. Mater. Chem. A* 2, 6064–6070. doi: 10.1039/C3TA14161F

Wu, S. D., Shi, F., Zhou, G., Zu, C., Liu, C., Liu, K., et al. (2018). Quantitative investigation of Polysulfide adsorption capability of candidate materials for Li-S batteries. *Energy Storage Mater*. 13, 241–246. doi: 10.1016/j.ensm.2018.01.020

Yang, Y., McDowell, M. T., Jackson, A., Cha, J. J., Hong, S. S., and Cui, Y. (2010). New nanostructured Li2S/Silicon rechargeable battery with high specific energy. *Nano Lett*. 10, 1486–1491. doi: 10.1021/nl100504q

Yang, Z., Guo, J., Das, K. S., Yu, Y., Zhou, Z., Abruna, D. H., et al. (2013). *In situ* synthesis of Lithium Sulfide–carbon composites as cathode materials for rechargeable Lithium batteries. *J. Mater. Chem. A* 1, 1433–1440. doi: 10.1039/C2TA00779G

Ye, F., Noh, H., Lee, J., Lee, H., and Kim, H. (2018). Li_2S/carbon nanocomposite strips from a low-temperature conversion of Li_2SO_4 as high-performance Lithium-Sulfur cathodes. *J. Mater. Chem. A* 6, 6617–6624. doi: 10.1039/C8TA00515J

Yu, M., Wang, Z., Wang, Y., Dong, Y., and Qiu, J. (2017). Freestanding flexible Li2S paper electrode with high mass and capacity loading for high-energy Li-S batteries. *Adv. Energy Mater*. 7:1700018. doi: 10.1002/aenm.201700018

Zhang, J., Shi, Y., Ding, Y., Peng, L., Zhang, W., and Yu, G. (2017). A conductive molecular framework derived Li2S/N,P-codoped carbon cathode for advanced Lithium–Sulfur Batteries. *Adv. Energy Mater*. 7:1602876. doi: 10.1002/aenm.201602876

Zhou, G., Tian, H., Jin, Y., Tao, X., Liu, B., Zhang, R., et al. (2017). Catalytic oxidation of Li2S on the surface of metal Sulfides for Li–S batteries. *Proc. Natl. Acad. Sci. U.S.A*. 114, 840–845. doi: 10.1073/pnas.1615837114

Zou, H., Gratz, E., Apelian, D., and Wang, Y. (2013). A novel method to recycle mixed cathode materials for Lithium Ion batteries. *Green Chem*. 15, 1183–1191. doi: 10.1039/C3GC40182K

Conflict of Interest Statement: The authors declare that the research was conducted in the absence of any commercial or financial relationships that could be construed as a potential conflict of interest.

Electronic Supplementary Information

Electrochemical potential window of battery electrolytes: the HOMO-LUMO misconception

Pekka Peljo*, Hubert H. Girault*

Laboratoire d'Electrochimie Physique et Analytique, École Polytechnique Fédérale de Lausanne, EPFL Valais Wallis, Rue de l'Industrie 17, Case Postale 440, CH-1951 Sion, Switzerland

1. Thermodynamic cycle to estimate the absolute redox potential of Fe(III)/(II) couple

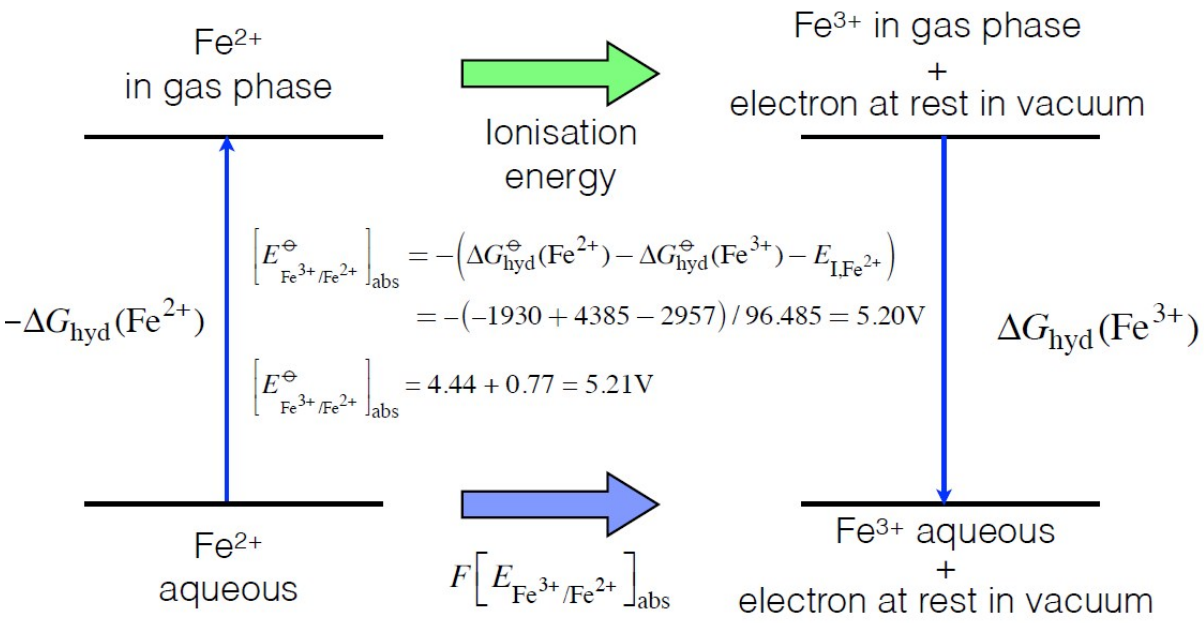

Figure S1. Thermodynamic cycle to estimate the absolute redox potential of Fe(III)/(II) couple considering the work to remove the solvation shell upon transfer of the Fe^{2+} into the gas phase, ionization energy and the solvation energy of Fe^{3+}, resulting in the absolute potential of 5.20 V.[1] The alternative approach is to utilize the standard redox potential of Fe(III)/(II) couple of 0.77 V *vs*. SHE and the definition of the SHE at the absolute vacuum scale of 4.44 V, resulting in the absolute potential of 5.21 V.

2. The correlation of the experimental ionization energies (HOMO) and tabulated standard reduction potentials of aqueous transition metal

Table S1.Experimental vertical ionization energies (VIE) of some hexaqua complexes of transition metal ions[2,3] and the corresponding standard oxidation and reduction potentials.[4]

Species	VIE, eV	Redox pair	E_{red}, V	Redox pair	E_{ox}, V
Ti^{3+}	7.05	Ti(III)/(II)	–0.369		
V^{3+}	8.41	V(III)/(II)	–0.255	V^{3+}/VO^{2+}	0.337
Cr^{3+}	9.48	Cr(III)/(II)	–0.407	Cr^{3+}/CrO_2	1.48
Cr^{2+}	6.76	Cr(II)/(0)	–0.913	Cr^{3+}/Cr^{2+}	0
Mn^{2+}	8.82	Mn(II)/(0)	–1.185	Mn^{3+}/Mn^{2+}	1.5415
Fe^{3+}	10.28	Fe(III)/(II)	0.771	$HFeO_4^-/Fe^{3+}$	2.07
Fe^{2+}	7.13	Fe(II)/(0)	–0.447	Fe^{3+}/Fe^{2+}	0
Co^{2+}	8.7	Co(II)/(0)	0.28	Co^{3+}/Co^{2+}	1.92
Ni^{2+}	9.45	Ni(II)/(0)	–0.252	NiO_2/Ni^{2+}	1.678
Cu^{2+}	9.65	Cu(II)/(I)	0.153	Cu^{3+}/Cu^{2+}	2.4

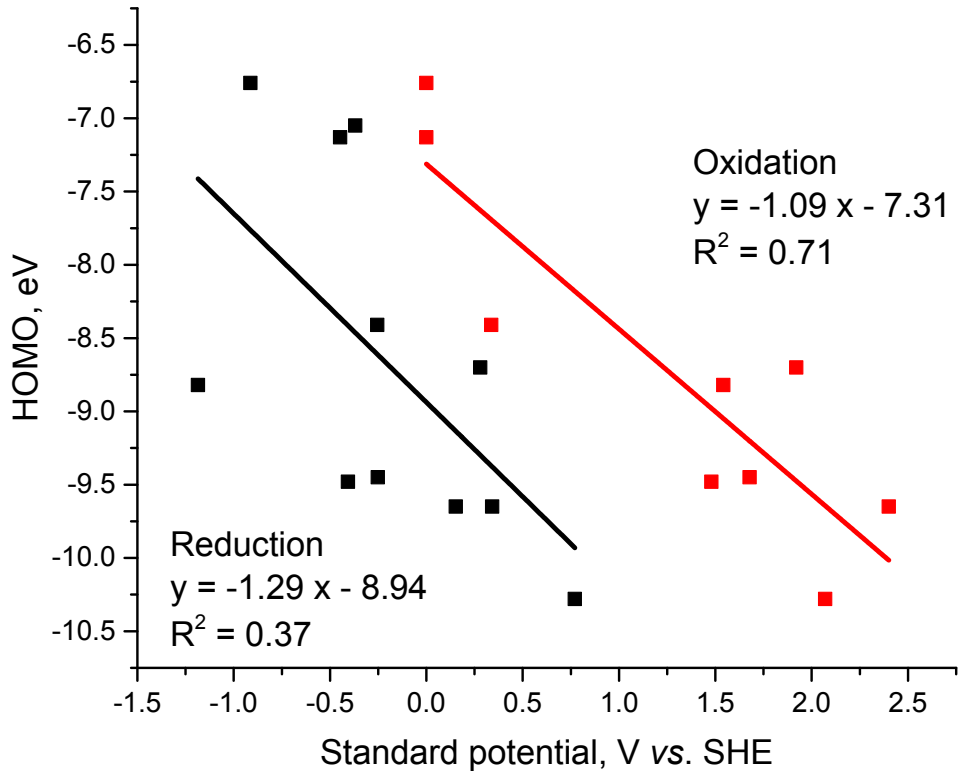

Figure S2. Correlation of the experimental HOMO energies (vertical ionization energy) and standard reduction potentials (black) and oxidation potentials (red) of the transition metals.

3. References

1 H. H. Girault, *Analytical and Physical Electrochemistry*, EPFL Press, Lausanne, 2004.

2 R. Seidel, S. Thürmer, J. Moens, P. Geerlings, J. Blumberger and B. Winter, *J. Phys. Chem. B*, 2011, **115**, 11671–11677.

3 D. Yepes, R. Seidel, B. Winter, J. Blumberger and P. Jaque, *J. Phys. Chem. B*, 2014, **118**, 6850–6863.

4 P. Vanýsek, in *CRC Handbook of Chemistry and Physics*, eds. W. M. Haynes, T. J. Bruno and D. R. Lide, Taylor and Francis Group, LLC, 96th edn., 2016, p. 5:79-88.